The summer pattern of the East Kamchatka Current from satellite altimetry data

Olga Trusenkova
Laboratory of physical oceanography
V.I. Il'ichev Pacific Oceanological
Institute FEB RAS
Vladivostok, Russia
ORCID:0000-0001-6756-5354

Elena Kustova
Laboratory of physical oceanography
V.I. Il'ichev Pacific Oceanological
Institute FEB RAS
Vladivostok, Russia
ORCID:0000-0001-9202-4613

***Abstract*— Using data from satellite altimetry, anomalies of surface velocity vectors in the area off the eastern Kamchatka from January 1, 1993, are expanded into complex (Hilbert) empirical orthogonal functions. Mode 1 covers 35-50% of the local variance within the East Kamchatka Current (EKC) path, manifesting variability on multiple timescales. The annual cycle is the most intense, while oscillations on the semiannual, quasi-biennial and 6-year timescales are statistically significant. Mode 1 intensifies twice a year: in winter from December through March and in summer from July through September. The winter pattern accounting for the southeastward-directed flow anomalies represents the EKC intensification in winter. The summer pattern accounting for the northeastward-directed flow anomalies represents the EKC weakening in summer. The EKC intensity in winter and summer generally matches each other, with the exception of 1998 and 2010 when the EKC was very weak in summer, while normal, i.e. no weak, no strong, in winter and 2018 when the EKC was strong in summer and normal to weak in winter. On the decadal timescale, the EKC was normal or weak in 1993–2002, strong to normal in 2003–2008, mostly normal in 2009–2014, and normal or strong in 2015–2023.**

Keywords*— *The East Kamchatka Current, satellite altimetry, Complex Empirical Orthogonal Functions, wavelet transform, semiannual, annual, quasi-biennial and 6-8-year timescales

I. Introduction

The East Kamchatka Current (EKC) is the cold western boundary current flowing southwestward in the western Bering Sea (northward of the Kamchatka Strait between the peninsula and Bering Island) and subarctic Pacific (southward of the Strait) from about 61° N to the southern tip of the Kamchatka Peninsula (see mean currents derived from daily satellite altimetry in Fig. 1) and continuing as the Kuril Current and Oyashio further south (see review in [1]). The coastline of the eastern Kamchatka undulates in a number of open bays, with matching bathymetry (Fig. 1, inset in the top left corner). Instability of the mean current combined with these topographic features results in formation of numerous mesoscale eddies documented in many studies, such as [2-6].

The primary forcing is the cyclonic wind stress curl prevailing over this area and, therefore the EKC intensifies in winter and weakens in summer (see review in [7]) and it is also subjected to the strong variability on interannual and decadal timescales [8, 9]. It has recently been shown that in summer, from July through September, a belt of low sea level anomalies is stretched out along the eastern Kamchatka coast [10], in line with the weakening of the EKC in summer.

The study was carried out as a part of the State Tasks No. 124022100079-4 and No. 124072200009-5 for POI FEB RAS.

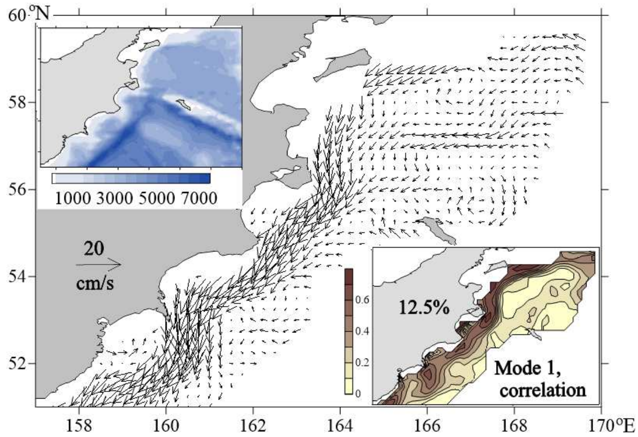

Fig. 1. Mean currents off Kamchatka; inset in the top left corner: bathymetry (m); inset in the bottom right corner: correlation between the Mode 1 temporal amplitude (CPCA1) and original current speed.

Recently, an area off the southeastern Kamchatka has attracted a lot of attention because of the harmful algae bloom in fall 2020 caused by *Karenia* species, resulting in severe damage to marine life [11]. From this viewpoint, understanding of the EKC variability is important for looking into possible pathways of algae movement.

Considering the above, the purpose of this study is to analyze the EKC variability using regular satellite data available for 30 years and to elucidate its statistical characteristics, with the emphasis on the summer patterns.

II. Data and Methods

The Copernicus Marine Service (CMEMS) gridded surface geostrophic velocities and velocity anomalies computed with respect to 1993–2012 are used in this study. Daily data from January 1, 1993, through June 7, 2023, with the spatial resolution of 0.25°, cover an area between 51° and 60° N within the EKC zone (Fig. 1). Many areas in the Bering Sea are ice-covered in winter and spring; however, the considered area is mostly free from fast ice, enabling multivariate data analysis throughout the year. Still, there are bins where sea ice can form and altimetry data are missing at some times. The bins where this happened at least once are excluded from the consideration, which mostly takes place in the north of the area (Fig. 1).

Vectors of velocity anomalies are expanded into empirical orthogonal functions (EOFs) in the complex form (the complex or Hilbert EOFs – CEOFs), with the zonal and meridional components representing real and imaginary parts, respectively. Prior to CEOF analysis, velocity components were low-pass filtered, with the cutoff period of 15 weeks. Elimination of high-frequency variability and the choice of the limited area around the EKC path (Fig. 1) enabled derivation of a reasonable leading mode. (Cutoff periods of 7–20 weeks were tried and the period of 15 weeks is chosen, as it provides a good balance between reasonable fraction of variance covered by the mode and seasonal variability retained.) The complex modes can be represented by amplitudes and phases of the spatial and temporal functions, i.e. CEOFs and complex principal components (CPCs), respectively.

Temporal variability is analyzed using wavelet transform with the Morlet mother wavelet of the 6-th order providing good resolution in the frequency (scale) domain. The statistical significance of the spectra is estimated with respect to the red noise at the 90% confidence level and the results are considered outside the cones of influence of edge effects [13]. The wavelet transform is also used for data filtering. Mathematical formulation is presented by [12] for the EOF analysis and by [13] for the wavelet analysis.

III. Results and Discussion

The complex Mode 1 derived from vectors of velocity anomalies covers 12.5% of the total variance. This does not seem much; however, correlation between the CPC amplitude (CPCA1; Fig.2a) and low-pass filtered current speeds (velocity modules) is equal to 0.4-0.5 and even exceeds 0.7 within the EKC path (Fig. 1, inset in the bottom right corner), corresponding to 35-50% of the local variance, thus justifying consideration of this mode. The lower modes are undistinguishable.

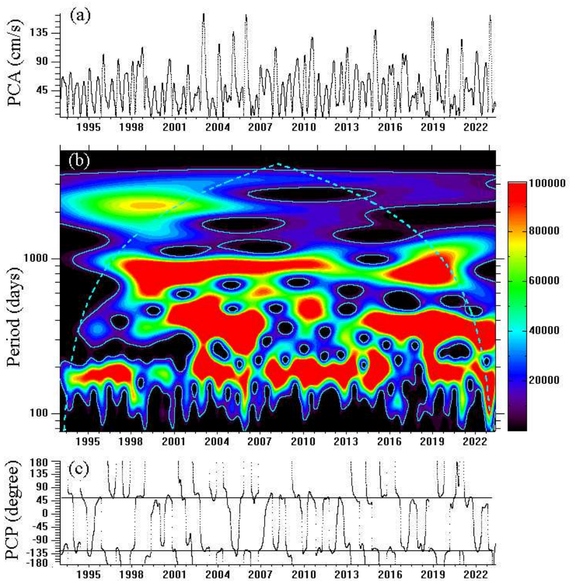

Fig. 2. CPCA1 (cm/s), (b) its wavelet spectrum (cm^2/s^2) and (c) Mode 1 temporal phase (CPCP1) (degree). Cones of influence of edge effects are shown by light blue dashed lines and contours of the 90% confidence level are light blue (b).

Mode 1 manifests rich temporal variability, as is seen in the CPCA1 wavelet spectrum where oscillations on the semiannual, annual, quasi-biennial and 6-8-year timescales are statistically significant throughout the record (Fig. 2b). In many years, there is also statistically significant power on the intra-annual timescales between 100 and 150 days. When averaging this spectrum on time, the annual oscillations are the most intense (not shown). Mean annual cycle of CPCA1 reveals two maxima in late January and August, the first one stronger than the second one (not shown). Therefore, Mode 1 intensifies twice a year. The annual oscillations weakened, while the semiannual ones intensified in 1993-2000 and 2007-2013 (Fig. 2b).

The CPC phase (CPCP1) defined between –180° and 180° (Fig. 2c) determines how the current directions related to the changes of Mode 1 in time. Preferential values, i.e. preferential current directions, can be seen in Fig. 2c where they are marked by horizontal lines. Frequency of occurrence for CPCP1 is estimated using histogram with 10-degree gradations. There are two strong peaks within the phase intervals of –110° to –130° and 50° to 70°, respectively (Fig. 3a), corresponding to the preferential values in Fig. 2c.

Monthly occurrences of CPCP1 taken within these two intervals show that the first one is the most frequent from December through March and practically zero from June through September and, therefore, represents a winter pattern. The second one is the most frequent from July through September and practically zero from December through March and, therefore, represents a summer pattern (Fig. 3b). Note that the seasonal maxima of CPCA1 in January and August agree with these months of high frequency. April, May, June, October and November are the transition months when CPCP1 gradually changes (Fig. 2c). As seen from the original daily maps, the circulation patterns are very changeable in the transition months (not shown).

Contributions of Mode 1 to the original currents corresponding to the winter and summer patterns are computed from CEOF1 and CPC1, with CPCP1 being equal to –120° and 60° for December – March and July – September, respectively, and CPCA1 averaged for these months. These contributions are flow anomalies; they represent currents of the opposite directions in winter and summer (Fig. 4). As expected, the winter pattern, corresponding to the southwestern current, accounts for the EKC strengthening in winter (Fig. 4a). Speeds of the mean altimetry-derived EKC (Fig. 1) are equal to 5–10 cm/s in the Bering Sea and 15–20 cm/s in the Pacific, while mean speeds

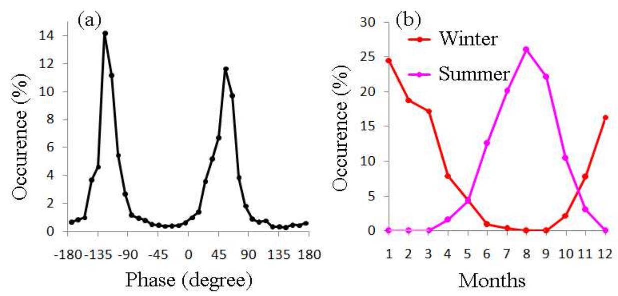

Fig. 3. (a) Net occurrence (%) of CPCP1, by gradations of 10°, and (b) monthly occurrence (%) for the gradation intervals of –110° to –130° (winter pattern, red curve) and 50° to 70° (summer pattern, magenta curve).

in winter are equal, on average, to 10–15 and 20–25 cm/s, respectively. In contrast, the summer pattern, corresponding to the northeasern current (Fig. 4b), accounts for the EKC weakening in summer, with the speeds equal, on average, to 2–7 cm/s in the Bering Sea and 10–15 cm/s in the Pacific.

Examples of daily currents in the events of the strong and weak Mode 1 when CPCA1 was high and low, respectively, are shown in Figs. 5 and 6. The winter pattern was strong in 2003 and weak in 1993 (Fig. 2a), which is clearly seen in the currents on January 1, 2003 (Fig. 5a) and on March 10, 1999 (Fig 5b), with the former stronger than the latter. As the summer pattern weakens the EKC, the current was weak when Mode 1 was strong, such as in 2010 (see an example of the original currents on August 14, 2010, in Fig. 6a), and the EKC was strong when Mode 1 was weak, such as in 2018 (see an example of the original currents on August 27, 2018, in Fig. 6b). At the times of the weak EKC the currents could be strong enough within eddies (Fig. 6a).

To determine years of the strong or weak patterns, yearly timeseries of CPCA1 averaged for December – March and July – September, respectively, for every year are computed. (December is attributed to the same year as January – March.) These timeseries are normalized using medians and mean deviations, as the short records of 30-31 counts are not normally distributed. Moreover, the sign of the summer timeseries is reversed, as the strong CPCA1 corresponds to the weak EKC and vice versa (Fig. 7). Years of the strong (weak) EKC are those when the values of the timeseries in Fig. 7 exceeded unity (were below minus unity) and they are summarized in Table 1; the other years are considered normal.

TABLE I. EXTREME YEARS OF THE EKC

Season	Year	
	The strong EKC	***The weak EKC***
Winter	2003, 2005, 2006, 2008, 2015, 2017, 2019, 2023	1993, 1994, 2000, 2001, 2002, 2011
Summer	2003, 2004, 2006, 2018, 2020	1996, 1997, 1998, 2000, 2007, 2009, 2010, 2013

The extremely strong EKC in winter when the normalized yearly mean CPCA1 exceeded 2 occurred in 2003 and 2019. There were also two years (1998 and 2010) of the extremely weak EKC in summer when the corresponding timeseries was below -2 (Fig. 7). The intensity of winter and summer patterns in the same year is mostly similar; the exceptions are 1998, 2010 and 2018 (in the latter case the EKC was strong in summer and normal in winter).

As seen from Fig. 7, there were time intervals differing in the EKC intensity. In 1993–2002 the EKC was weak or normal, strengthening from 2000 to 2003, and in 2003–2008 the EKC was strong or normal. This variability is consistent with that reported by [8]. The EKC was mostly normal in 2009–2014, intensified from 2014 to 2019 and was normal or strong in 2015–2023. Note that the EKC intensification during the last decade was reported for April and May [14]. These changes can be referred to the 15–16-year timescale, which is not evident in the spectrum (Fig. 2b) due to the insufficient record length of 30–31 years.

It is well known that the cyclonic circulation in the subarctic North Pacific is forced by cyclonic wind stress curl which intensifies in winter. To check linkages with atmospheric processes, the North Pacific Index (NPI), the area-weighted mean sea level pressure over the region 30° to

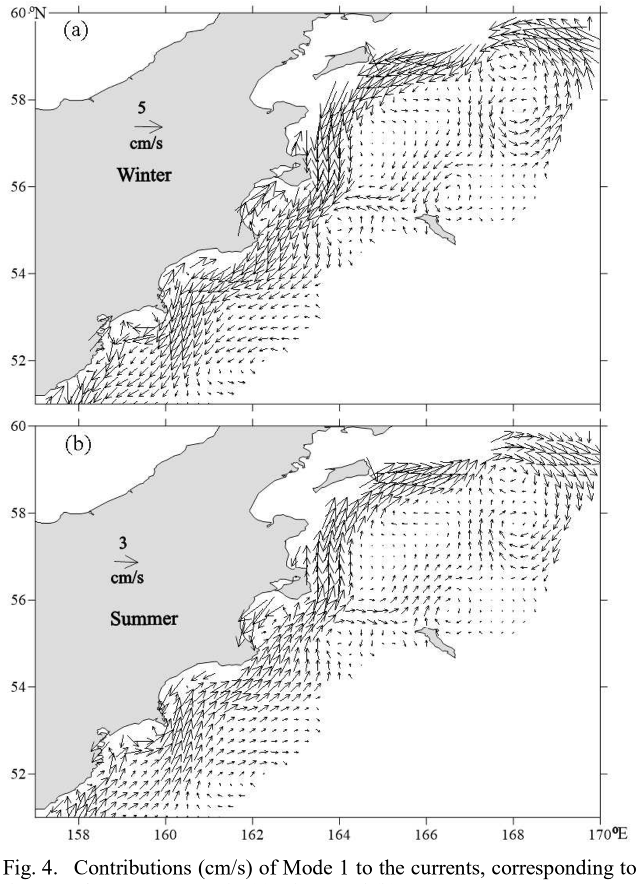

Fig. 4. Contributions (cm/s) of Mode 1 to the currents, corresponding to the most frequent CPCP1 in (a) winter and (b) summer.

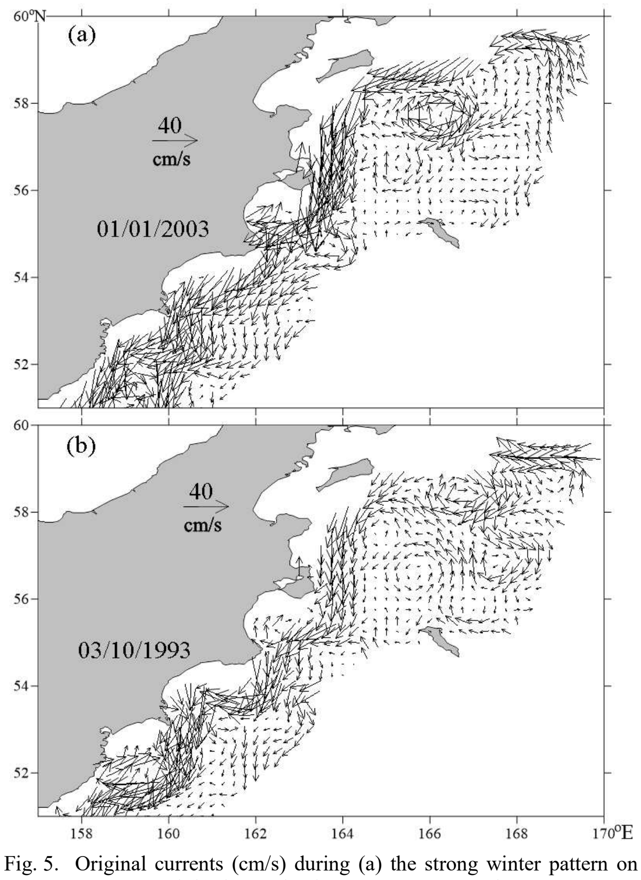

Fig. 5. Original currents (cm/s) during (a) the strong winter pattern on January 1, 2003, and (b) the weak winter pattern on March 10, 1993.

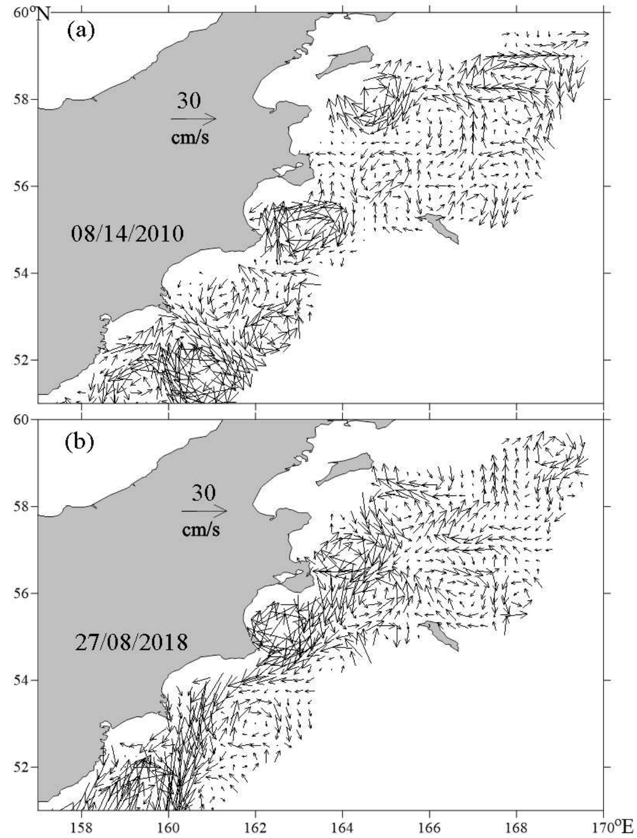

Fig. 6. Original currents (cm/s) during (a) the strong summer pattern on August 14, 2010, and (b) the weak summer pattern on August 27, 2018.

65° N, 160° E to 140° W [15] was applied. NPI substantially drops in winter when the Aleutian Low and wind over North Pacific intensify. (The lower NPI, the stronger the Aleutian Low.) Correlation between CPCA1 and NPI is equal to –0.4, due to the CPCA1 winter maximum, implying forcing of the EKC in the entire area between 51° and 60° N by wind stress curl. There is no statistically significant linkage between CPCA1 and NPI on interannual timescales; however, zonal or meridional shifts of the Aleutian Low, occurring on interannual timescales, probably do not alter NPI but result in changes of wind off Kamchatka and the EKC forcing, as discussed by [8]. Linkages of the EKC with wind stress curl over the subarctic North Pacific will be a subject of future research.

It is worth noting that the summer pattern occurs from July through September, in the time of the strongest surface heating and baroclinicity. On the other hand, the alongshore belt of negative sea level anomalies reported by [10] for summer, which is consistent with the EKC weakening, can be induced by upwelling; upwelling favorable southerly winds are frequent off Kamchatka in summer.

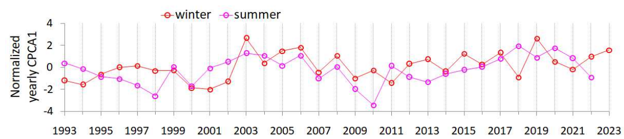

Fig. 7. Normalized yearly mean CPCA1 for winter (red curve) and summer (magenta curve); CPCA1 for summer is taken with the opposite sign. Positive (negative) values above unity (below minus unity) correspond to the strong (weak) EKC.

IV. CONCLUSION

In this study data from satellite altimetry for the period from January 1, 1993, onwards are used for multivariate analysis of surface currents in the area off the eastern Kamchatka coast in both Bering Sea and subarctic northwestern Pacific. Anomalies of the surface velocity vectors are expanded to CEOF and the leading Mode 1 covering 35-50% of the local variance within the EKC path manifests variability on multiple timescales which are estimated using wavelet transform. As expected, in the temporal variability of Mode 1 the annual timescale is the most intense; however, the semiannual, quasi-biennial and 6 year timescales are also statistically significant throughout the record.

The CEOF Mode 1 intensifies twice a year: in winter from December through March and in summer from July through September, with the winter maximum, on average, stronger than the summer one. The winter pattern accounting for the southeastward-directed flow anomalies represents the EKC intensification in winter and the summer pattern accounting for the northeastward-directed flow anomalies represents the EKC weakening in summer, which is in line with earlier findings [1, 7]. However, if wind is considered as the primary forcing of the EKC [8, 9] it is not clear why this current is the weakest in July – September, as the wind weakens in April and strengthens again in September. Probably another cause of this timing should be also considered, such as hydrodynamic instability in the period of the strongest pycnocline (July – September). This suggestion should be verified by future research.

Years of the strong and weak EKC are detected. The EKC intensity was similar in winter and summer of the same year, with the exception of 1998 and 2010 when the EKC was very weak in summer, while normal, i.e. no weak, no strong, in winter, and 2018 when the EKC was strong in summer and normal to weak in winter. On the decadal timescale, the EKC was normal or weak in 1993–2002, strong to normal in 2003–2008, mostly normal in 2009–2014, and normal or strong in 2015–2023. The EKC changes in 1993–2008 are in line with the earlier findings by [8]. Therefore, 15–16-year variability manifests itself in the EKC intensity, which is not evident from the spectral analysis due to relatively short record.

ACKNOWLEDGMENT

The authors thank Drs. M. Uleisky and M. Budyansky for preparation of altimetry data. We acknowledge Drs. C. Torrence and G.P. Compo for their free software for wavelet analysis. We are grateful to Dr. E. Ustinova for the careful reading of the manuscript and valuable comments.

REFERENCES

[1] K.K. Kivva et al. PICES special publication 7. Marine Ecosystems of the North Pacific Ocean 2009-2016: Region 16 (Western Bering Sea). Sidney, BC, Canada: North Pacific Marine Science Organization, 2023.

[2] H. Solomon and K. Ahlnäs, “Eddies in the Kamchatka Current,” Deep Sea Research, vol. 25, no. pp. 403–410, April 1978.

[3] F.F. Khrapchenkov, “Issledovaniye vikhrey u poberezhya Kamchatki letom 1985 g. (Field study of eddies near the Kamchatka coast in the summer of 1985),” Oceanology, vol. 27, pp. 391–396, June 1987 [in Russian].

[4] P.J. Stabeno, R.K. Reed, and J.E. Overland, “Lagrangian measurements in the Kamchatka Current and Oyashio,” J. Oceanogr., vol. 50, pp. 653–662, November 1994.

[5] K.A. Rogachev, and N.V. Shlyk, “Characteristics of the Kamchatka current eddies,” Russ. Meteorol. Hydrol., vol. 44, pp. 416–423, June 2019. [Meteorologija i Gidrologija, no. 6, 70-79, June 2019].

[6] N.M. Vakulskaya, V.A. Dubina, and V.V. Plotnikov, “Vikhrevaya struktura Vostochno-Kamchatskogo techeniya po sputnikovym nablyudeniyam (Eddy structure of the east Kamchatka Current according to satelline observations),” in Physics of Geospheres, Proc. XI All-Russia Symposium, September 9-14, 2019, Vladivostok, Russia, pp. 73-81 [in Russian].

[7] T. Ono et al. PICES special publication 7. Marine Ecosystems of the North Pacific Ocean 2009-2016: Region 23 (Western Subarctic Gyre). Sidney, BC, Canada: North Pacific Marine Science Organization, 2022.

[8] G.V. Khen and A.N. Zaochny, “Izmenchivost' raskhoda Kamchatskogo techeniya i okeanologicheskikh parametrov v Kamchatskom prolive (Variability of the Kamchatka Current transport and water properties in the Kamchatka Strait)”, Izvestiya TINRO, vol. 158, pp. 247–260, May 2009.

[9] G.V. Khen, E.O. Basyuk, N.S. Vanin, and V.I. Matveev, “Hydrography and biological resources in the western Bering Sea”, Deep-Sea Research II, vol. 94, pp. 106–120, October 2013.

[10] K.E. Shevchenko and K. Romanov, “O znachenii prilivnoy korrektsii dlya rascheta srednikh poverkhnostey urovnya morya po dannym sputnikovoy al'timetrii IMMOAD SSHA (On the importance of tidal correction for calculation of mean sea level surfaces from IMMOAD SSHA satellite altimetry data)”, Current problems in the remote sensing of the Earth from the space, vol. 20, no. 6, pp. 80-91, November 2023.

[11] T.Y. Orlova, A.I. Aleksanin, E.V. Lepskaya et al., “A massive bloom of Karenia species (Dinophyceae) off the Kamchatka coast, Russia, in the fall of 2020”, Harmful Algae, vol. 120, 102337, December 2022.

[12] A. Hannachi, “Complex/Hilbert EOFs,” in Patterns Identification and Data Mining in Weather and Climate. Springer Atmospheric Sciences. Springer, Cham, 2021, pp. 91-115.

[13] C. Torrence and G. P. Compo, “A practical guide to wavelet analysis,” Bull. Am. Meteorol. Soc., vol. 79, pp.61–78, January 1998.

[14] O.B. Tepnin, “Izmenchivost' gidrologicheskih uslovij v mestah neresta vostochnokamchatskogo mintaja (*Gadus Chalcogrammus*) (Variability of hydrological conditions at spawning sites of east Kamchatka walleye Pollock (*Gadus Chalcogrammus*))”, The researches of the aquatic biological resources of Kamchatka and the north-west part of the Pacific Ocean, vol. 66, pp. 79-93, July 2022 [in Russian].

[15] G. Trenberth and J.W. Hurrell, “Decadal atmosphere-ocean variations in the Pacific”, Climate Dynamics, vol. 9, pp. 303–319, April 1994.